Band offsets and transport mechanisms of hydrogenated nanocrystalline silicon/crystalline silicon heterojunction diode: Key properties for device applications

J. J. Lu, J. Chen, Y. L. He, and W. Z. Shen[a)]
Laboratory of Condensed Matter Spectroscopy and Opto-Electronic Physics, Department of Physics, Shanghai Jiao Tong University, 1954 Hua Shan Road, Shanghai 200030, People's Republic of China

(Received 11 May 2007; accepted 24 July 2007; published online 17 September 2007)

We have studied the electrical properties of hydrogenated nanocrystalline silicon/crystalline silicon heterojunction diode, focusing on the band offsets and electron transport mechanisms. Capacitance-voltage (C-V) analysis reveals that the band discontinuity mainly exists on the valence-band side, and an interface charge density on the order of 10^{11} cm^{-2} is estimated via the numerical C-V matching technique. Temperature- and bias-dependent transport mechanisms have been clarified by dark current-voltage-temperature measurements, and the extracted parameters indicate a transition from nontunneling to tunneling dominant transport from 350 to 20 K. © *2007 American Institute of Physics*. [DOI: 10.1063/1.2779267]

I. INTRODUCTION

Heterojunction (HJ) devices have widespread applications in modern solid state electronics, including transport across the interface [

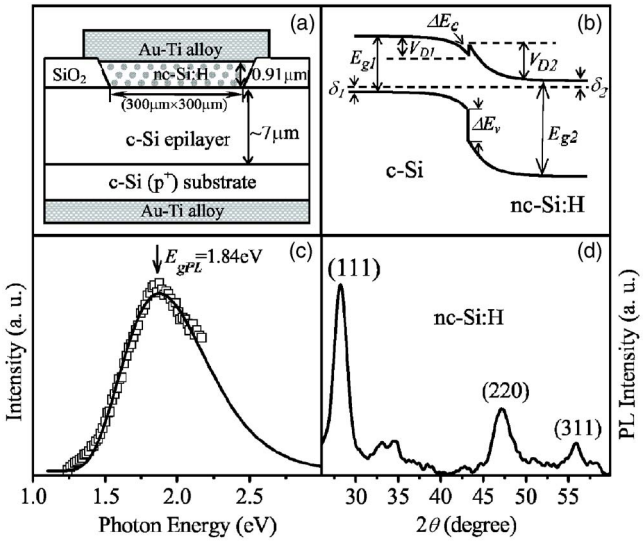

FIG. 1. (a) Cross-sectional view of the nc-Si:H(n)/c-Si(p) HJ diode with geometric parameters. (b) Schematic energy band diagrams of nc-Si:H(n)/c-Si(p) heterostructure. (c) PL of the nc-Si:H film. Empty squares: experimental data; solid curve: theoretical fitting result. (d) XRD spectrum of the nc-Si:H film.

$\times 300\ \mu m^2$) to accommodate the nc-Si:H deposited in the following step. The n-type nc-Si:H layer was prepared in a rf (13.56 MHz) capacitive coupled plasma enhanced chemical vapor deposition (PECVD) system with a power density about 0.6 W cm^{-2} and dc bias (−200 V) stimulation. A strongly hydrogen diluted silane, i.e., 1% SiH_4 diluted with H_2, was employed as the reactant gas source. Doping was realized by adding PH_3 to the mixed reactant gas, and the doping ratio C_p which is defined as PH_3/SiH_4 was set at 0.1 vol %. The thickness of the nc-Si:H layer was 0.91 μm, which was determined by a surface profiler on a dummy wafer. Finally, Ohmic contacts were made on both the c-Si substrate and the nc-Si:H top layer by evaporating Au–Ti alloys in vacuum. Figure 1(a) schematically shows the structure of the HJ device that we used to perform electrical characterizations.

B. Characterization

X-ray diffraction (XRD) and PL spectrum at room temperature were employed to test the semifinished HJ diode without the Au–Ti alloy electrodes. The XRD measurement was performed on a Rigaku Dmax-rc instrument in the standard θ-2θ configuration with a Cu $K\alpha_1$ radiation (1.5406 Å), and the PL spectrum was obtained from a Jobin Yvon LabRAM HR 800 UV micro-Raman spectrometer using 514.5 nm line from an Ar^+ laser. Room temperature C-V characterization of the packaged nc-Si:H(n)/c-Si(p) HJ diode was carried out on a computer controlled C-V system, which consisted of an Agilent 4284A *LCR* meter together with the external voltage bias fixture accessory (model 16065a), a Keithley 2400 source-meter functioning as the voltage source, and a Keithley 2182 voltage meter acting as the voltage meter. For the temperature-dependent C-V measurements (10–300 K), an Oxford Instruments superconductive magnet system, which simultaneously provided the low temperature and good electromagnetic shielding environment, was utilized to work with the above mentioned C-V setup. Additional short/open/load corrections of the whole C-V system were performed to ensure the validity of the test results. Lastly, the temperature-dependent dark current-voltage measurements of the packaged HJ diode were done on a Keithley 2400 source-meter (sweeping mode) in a Janis closed-cycle refrigerator system with temperature ranging from 20 to 350 K.

III. RESULTS AND DISCUSSION

The band discontinuity of the semiconductor heterostructure has been recognized as the fundamental problem of HJ devices, and a number of electrical and optical techniques have been developed to determine the band offset parameters, in which C-V analysis has been widely[18] used in various silicon based anisotype HJs, such as a-Si:H/c-Si,[19] SiGe/c-Si,[20] and a-SiGe:H/c-Si.[21] In order to obtain correct results from the C-V data, prerequisite material parameters of nc-Si:H should be accurately provided first of all. Compared with its well-known crystalline counterpart, the hydrogenated nanocrystalline Si exhibits quite different physical properties, especially in the band gap, the static dielectric constant, and the effective mass of the electron, which are critical values in yielding reliable band structure for nc-Si:H/c-Si HJ [as schematically shown in Fig. 1(b)] from a successful C-V analysis.

For the band gap parameter, it is generally accepted that owing to the breakdown of translation invariance, the QCE in nc-Si:H opens up the band gap and relaxes the **k**-conservation rule for radiative transitions, giving rise to the visible PL as shown in Fig. 1(c) for our diode without the Au–Ti alloy electrodes. The band gap can be directly read from the PL profile ($E_{g\mathrm{PL}}$=1.84 eV), which is different from that in bulk c-Si (1.12 eV) and in completely amorphous silicon films (1.7 eV). As for the static dielectric constant of the nc-Si:H, there have been a number of studies[22–24] on the reduction of the dielectric constants of nanoscale systems from their bulk values. It was recently[24] argued that the reduction is not due to the opening of the band gap induced by the QCE, but the breaking of polarizable bonds at the surface. According to Wang and Zunger,[22] a size-dependent static dielectric constant of nc-Si considering the screening effect is suitable for our discussion:

$$\varepsilon_{nc\text{-Si}} = 1 + \frac{\varepsilon_{\text{bulk-Si}} - 1}{1 + (1.38/D)^{1.37}}, \tag{1}$$

where $\varepsilon_{\text{bulk-Si}}$ is the dielectric constant of bulk crystalline silicon, and D is the nc-Si size in the unit of nanometers, which can be obtained from XRD measurement [Fig. 1(d)] using the Scherrer formula[25]

$$D = \frac{K\lambda}{w\cos(\theta)}, \tag{2}$$

where K is approximately 1, λ is the wavelength of the x rays, w is the width of the band after correcting the instrumental contribution, and θ is the Bragg angle of the diffracting planes. The good quality of the Si nanocrystals is indi-

cated by the relatively sharp and symmetric (111) peak in Fig. 1(d), together with two broad [(220) and (311)] structures. The calculated average grain size from XRD is 4.8 nm, and it obeys a log-normal distribution with size dispersion around 4%,[10] which is obtained from the fitting result of the PL spectrum [solid curve in Fig. 1(c)] by the Islam and Kumar model.[26] The corresponding calculated static dielectric constant of nc-Si is 10.1. However, the effective dielectric constant for the nc-Si:H thin film should take the background amorphous silicon into consideration. Defining the crystalline ratio r of the nc-Si:H film (~55% from the Raman analysis[10]), the average is simply given by[24]

$$\varepsilon_{\text{eff}} = r\varepsilon_{\text{nc-Si}} + (1-r)\varepsilon_{\text{a-Si}} \tag{3}$$

The resulted effective dielectric constant for the nc-Si:H thin film is 10.9. In addition, compared with the crystalline silicon, the effective mass of the electron of nc-Si:H is greatly reduced due to the strain-induced effect. For our HJ sample, by the aid of the magnetic-field-dependent Hall effect measurement,[11] the value can be extracted from the generalized Drude model as $0.35m_0$, where m_0 is the free-electron mass.

With the above parameters, C-V spectrum can now be employed to determine the energy band structure of the HJ. It is well known that the capacitance of the ideal anisotype HJ under reverse bias can be modeled by the Anderson model[27] under the electron affinity rule and the depletion approximation. For the nc-Si:H(n)/c-Si(p) HJ diode, the junction capacitance is given by

$$C^2 = \frac{q\varepsilon_1\varepsilon_2 N_1 N_2}{2(\varepsilon_1 N_1 + \varepsilon_2 N_2)(V_{\text{bi}} - V)}, \tag{4}$$

where q is the electronic charge, C is the junction capacitance per unit area, N and ε are the net free-carrier concentration and dielectric constant with subscripts 1 and 2 referring to c-Si [(111) epitaxial layer] and nc-Si:H, respectively, V_{bi} is the built-in voltage (i.e., diffusion potential), and V is the applied reverse voltage bias. Knowing the junction area and the material parameters of nc-Si:H as discussed above, one can linearly fit the $1/C^2 \sim V$ curve and calculate V_{bi} and N_2 from the interception of the V axis and the slope of the line, respectively. For our anisotype HJ, it is relatively straightforward to obtain the conduction-band discontinuity ΔE_C and valence-band discontinuity ΔE_V through[18]

$$\Delta E_C = qV_D - E_{g1} + \delta_1 + \delta_2, \tag{5a}$$

$$\Delta E_V = E_{g2} - (qV_D + \delta_1 + \delta_2), \tag{5b}$$

where E_g is the forbidden band gap and δ is the difference in energy between the Fermi level and the valence-band maximum or the conduction-band minimum for different sides of the junction, as depicted in Fig. 1(b). Furthermore, δ_1 and δ_2 can be calculated via

$$\delta_1 = kT \ln\left(\frac{N_1}{N_V}\right), \tag{6a}$$

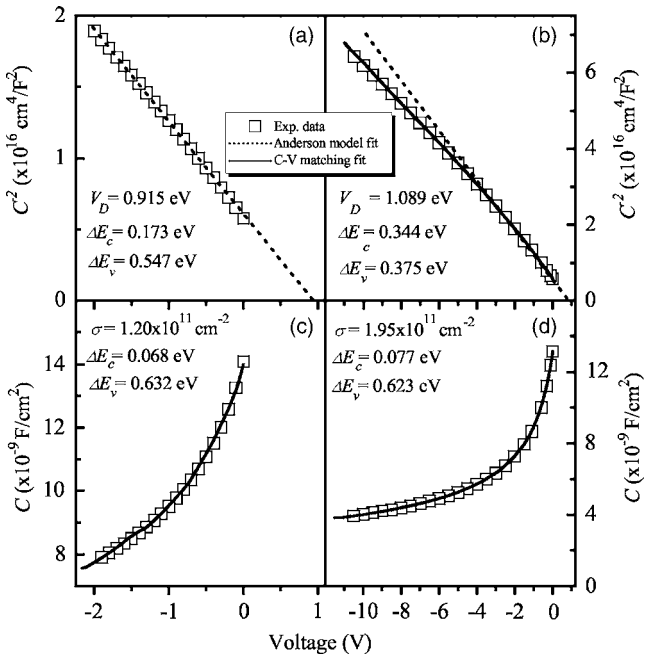

FIG. 2. Anderson model fitting $1/C^2 \sim V$ results (dashed lines) for different reverse bias voltage spans from (a) 0 to −2 V and (b) 0 to −5 V. Simulated C-V matching results (solid curves) are displayed in (c), (b), and (d) with the bias range of 0 to −2 and 0 to −10 V, respectively. Empty squares: experimental C-V data.

$$\delta_2 = kT \ln\left(\frac{N_2}{N_C}\right), \tag{6b}$$

where kT is the Boltzmann energy at temperature T, and N_V and N_C refer to the effective valence-/conduction-band density of states for c-Si and nc-Si:H, respectively, which are functions of the reduced effective mass of the electron and of T.

Figure 2(a) illustrates the fitted $1/C^2 \sim V$ curve (dashed line) for the reverse bias voltage span from 0 to −2 V by using the Anderson model. The good linear fit of the experimental $1/C^2 \sim V$ results for the reverse bias ranging from 0 to −2 V confirms that the formed nc-Si:H/c-Si HJ is an abrupt one. However, as shown in Fig. 2(b), it is found that with the increase of the reverse bias from −2 to −5 V, the linearity of the $1/C^2 \sim V$ curve deteriorates. If we simply apply the Anderson model to these two different voltage spans, i.e., 0 to −2 V and 0 to −5 V, discrepancy in the deduced built-in voltages will occur [see linear fitting dashed lines in Figs. 2(a) and 2(b)], and the calculated band offsets will exhibit considerable difference [see the values listed in Figs. 2(a) and 2(b)]. Similar nonlinearity issue has also been reported by Kamjoo *et al.*[20] with the SiGe/c-Si HJ, and it was argued that interface charges can contribute to a parasitic capacitance that acts in parallel with the depletion capacitance. Therefore, the resulting equivalent capacitance would be larger than that of the ideal depletion capacitance. Moreover, interface defects will also invoke the discontinuity in the electric field, which can drastically affect the band bending. However, these arguments should be further examined by the capacitance-frequency (C-f) spectrum. Figure 3(a) demonstrates a small variance of C-V curves under four different frequencies, ruling out the possible impurity contami-

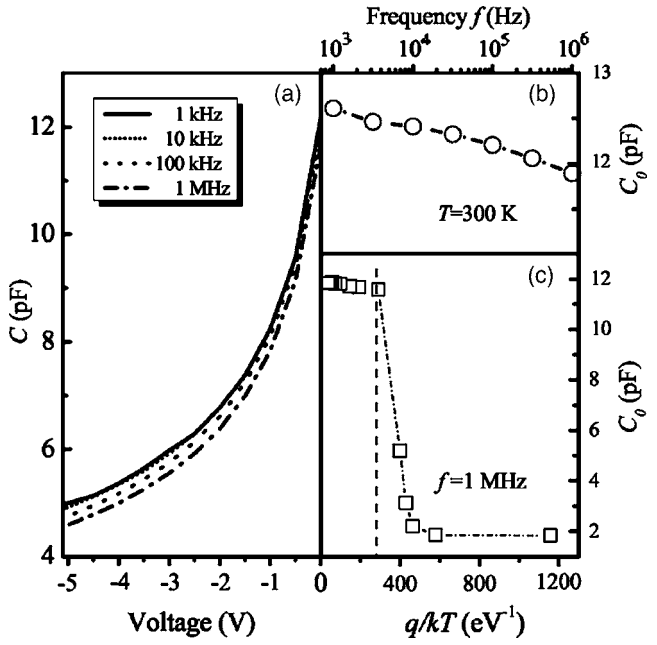

FIG. 3. (a) *C-V* dependence at four different frequencies. (b) Zero bias junction capacitance C_0 over a wide range of frequencies from 1 kHz to 1 MHz at 300 K. (c) Relationship between C_0 and q/kT at the frequency of 1 MHz. The dashed curves in (b) and (c) are guides for eyes.

nations which might be introduced during the growth of nc-Si layer.[28] Figure 3(b) also illustrates the zero bias junction capacitance C_0 over a wide range of frequency span from 1 kHz to 1 MHz. The increase of C_0 at low frequency may originate from the heterointerface defects,[29] however, the small change in value (less than 10% increase) excludes the influence induced by heavy interface defects.

Evidenced by the frequency insensitive *C-f* results, our consideration is narrowed down to the existence of static interface charges, which can be introduced by fundamental and technological sources. For our nc-Si:H$(n)/c$-Si(p) HJ diode, they may come from chemical bonds across the heterointerface and the structural imperfections of the amorphous silicon lying in between the nc-Si nanodots. In dealing with the interface charge density σ, self-consistent calculations are often utilized to simulate the *C-V* responses of heterostructures or even quantum wells. Although physically sound, the self-consistent calculations of Poisson's and Schrödinger's equations are numerically complicated to implement; and furthermore, the information provided by the experimental *C-V* data has not been fully exploited during the simulation process. Recently, Nemirovsky *et al.*[30] have proposed a *C-V* matching methodology to simultaneously determine the band discontinuities and interface charge densities of the HJs. The analysis is based on the fact that a given *C-V* measurement is actually a vector of capacitance values for a set of applied voltage values. For each voltage value of the *C-V* measurement, there is a separate set of three cardinal equations: the band lineup equation, the charge balance equation, and the capacitance equation, which can be written as follows:

$$E_{\mathrm{FC}_1} - E_{\mathrm{FC}_2} - \Delta E_C - qV = q[V_{D2}(V) - V_{D1}(V)], \tag{7}$$

$$Q_1[V_{D1}(V)] + Q_2[V_{D2}(V)] + q\sigma = 0, \tag{8}$$

$$\frac{1}{C_t} = \frac{1}{C_1[V_{D1}(V)]} + \frac{1}{C_2[V_{D2}(V)]}, \tag{9}$$

where the subscripts 1 and 2 refer to the *c*-Si side and nc-Si:H side, respectively, E_{FC_1} and E_{FC_2} are the differences between the quasi-Fermi energy levels and the respective conduction-band levels, Q_1 and Q_2 are the total charges per unit area on each side of the HJ, C_1 and C_2 are the total capacitances per unit area on each side of the HJ, and C_t is the total capacitance per unit area of the HJ device. Detailed expressions for E_{FC}, Q, and C can be found in Ref. 30. There are altogether four unknown variables defined in Eqs. (7)–(9), i.e., ΔE_C, σ, V_{D1}, and V_{D2}, the latter two of which are band bendings on each side of the heterointerface varying with the applied voltage V, as shown in Fig. 1(b). The basic idea behind the *C-V* matching method is to use the additional information contained in the whole ensemble of sets of equations, in order to simultaneously find ΔE_C and σ that match optimally to the entire *C-V* data, which in essential is a regression analysis process.

Figures 2(b)–2(d) present the simulated *C-V* relations (solid curves) by using the above *C-V* matching approach, which are in good agreement with the experimental results. The yielded values of ΔE_c, ΔE_v, and σ are also listed in the figure, indicating a very small conduction-band offset, and the band discontinuity mainly exists on the valence-band side, which is in agreement with the previous reports on the *a*-Si:H/*c*-Si heterostructure.[31,32] Comparing Fig. 3(c) with Fig. 3(d), the values of band offsets are consistent even with the increase of the reverse bias from −2 to −10 V, while the derived interface charge density increases with larger reverse bias, but still stays on the order of 10^{11} cm^{-2}, which is relatively low compared with the much higher interface density of states in *a*-Si:H/*c*-Si HJ.[32] It implies that although nc-Si:H layer was deposited on the densest (111) growth plane of the epitaxial crystalline silicon, only part of the unsaturated and hanging bonds was left at the nc-Si:H/*c*-Si heterointerface, thanks to both the passivation effect by the great amount of diluting hydrogen introduced during the plasma processing and the high crystalline ratio (~55%) of the nc-Si:H film. The relatively low interface defect density has also been confirmed by the former frequency insensitive *C-V* results. By analogy with *a*-Si:H/*c*-Si solar cells,[33] an intrinsic layer of nc-Si might be inserted between the nc-Si:H and *c*-Si to further reduce the fixed interface charge density and improve the conversion efficiency of HJ solar cells. As for the small increase of the interface charge density with larger reverse bias, it can be accounted for by considering the width increase of the depletion region when raising the reverse bias, which will take in more nc-Si dots surrounded by the spherical "microheterointerfaces," and the contributed interface charges will in effect build up and bend the originally linear $1/C^2 \sim V$ curve. To minimize the effect of the bias-dependent interface charges on the band discontinuity, we recalculate the band offset values using the above *C-V* matching procedure in the bias range from 0 to −0.5 V, corresponding to the maximum depletion region width of

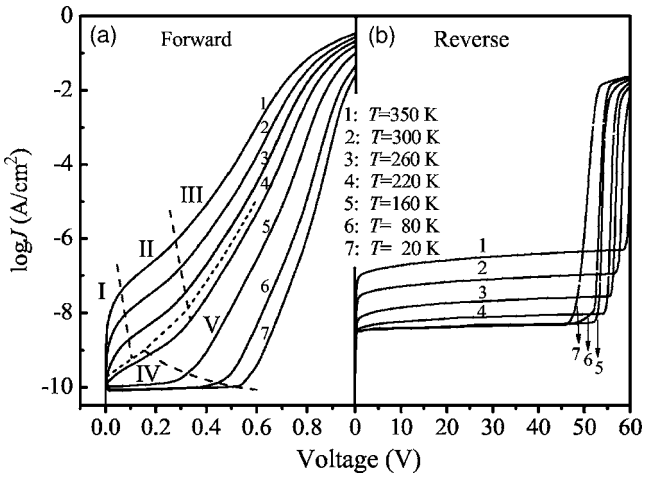

FIG. 4. (a) Forward and (b) reverse current density-voltage characteristics of nc-Si:H(n)/c-Si(p) HJ diode at seven representative temperatures.

~6 nm on the nc-Si:H side, and the obtained ΔE_c, ΔE_v, and σ are 0.061 eV, 0.639 eV, and 0.95×10^{11} cm^{-2}, respectively, which again confirms the near-zero conduction-band offset.

In addition, to better understand the capacitance response of the nc-Si/c-Si HJ diode under a wide range of temperatures, the zero bias junction capacitance C_0 was measured against the temperature from 300 down to 10 K. As shown in Fig. 3(c), a small monotonic decrease of the capacitance with decreasing temperature is demonstrated from 300 to 40 K, which is due to the increase of the built-in potential and thus the width of the space charge region, owing to the statistical shift of the Fermi level in both c-Si and nc-Si:H with decreasing temperature. However, a sharp reduction of C_0 is observed at 40 K, below which the classical depletion region limited model of junction capacitance becomes invalid, and the capacitance-voltage relation (not shown in the figure) approaches a constant value of about 2 pF at 10 K. This phenomenon corresponds well with the latter discussed dark J-V behavior at low temperatures, which in principle reflects that the electrons are confined in the nanodots to respond to the width variance of the depletion region.

Having yielded a clear band structure by the above C-V analysis, transport characteristics of the HJ diode as a practical device still need to be clarified based on experimental results. Forward and reverse dark J-V measurements of our HJ diode were carried out over a wide temperature range from 20 to 350 K, among which seven representative J-V curves for specific temperatures are illustrated in Fig. 4. At a first glance, the HJ diode exhibits a good rectifying effect with a rectifying ratio of about 7.6×10^2 at 300 K, and a hard breakdown happens when the reverse bias exceeds ~58 V. Moreover, by carefully inspecting Fig. 4(a), the forward J-V curves experience several transitions due to different dominant transport mechanisms under different biases and temperature conditions. Accordingly, for the high temperature region (from 220 to 350 K), three distinct zones, "I," "II," and "III," are designated for the low (0–0.1 V), medium (0.1–0.3 V), and high (0.3–0.8 V) voltage regimes, among which zone I is normally considered in a thermal equilibrium of the operating HJ. As for the low and medium temperature regions (from 20 to 220 K), zones "IV" and "V" are specified on the basis of turn-on voltages. All of the zones mentioned above are separated with dashed lines, as shown in Fig. 4(a).

To distinguish one transport mechanism from the others, we employ the well-known general junction rectification model[14] to describe the relation between the current and the applied forward voltage, which can be written as

$$J = J_0[\exp(AV) - 1], \tag{10}$$

where A is a coefficient defined by

$$A = \frac{q}{\eta kT}, \tag{11}$$

where k is the Boltzmann constant and η is the ideality factor. J_0 in Eq. (11) is the saturation current density defined by

$$J_0 \propto \exp\left(-\frac{E_{\mathrm{ac}}}{kT}\right), \tag{12}$$

where E_{ac} is the activation energy. As can be seen from the above three equations, these parameters are a function of both the transport mechanism, characterized by η and temperature. Therefore, both A and the properties of the ideality factor can elucidate the dominant transport mechanism. If the current is limited by the diffusion process, then $\eta=1$. However, if the transport is controlled by the carrier recombination process within the depletion region, $\eta=2$ is expected, and E_{ac} is equal to $E_g/2$, in which E_g is the energy gap in the zone where recombination takes place. The classical value 2 is obtained for only one recombination level at the exact midgap with identical capture cross sections for electrons and holes. In amorphous semiconductors where there is a continuous distribution of traps in the gap, $\eta<2$ should be anticipated. What is more, if the current is dominated by the tunneling process, the term A should be temperature independent. It must be emphasized that all the transport process may be occurring at the barrier of the HJ, whereas the measured current density will usually be dominated by only one of them. In addition, we have also neglected the influence imposed by the HJ interface charges, which indeed have no effect on the diffusion-limited current.[34]

Using the above general junction rectification model, we may attribute zones II and III to the recombination- and diffusion-dominant transport mechanisms, respectively, which is supported by the fitting results in Figs. 5(a) and 5(b). According to the slope of the fitted parameter A, Fig. 5 has been divided into three temperature regions (see vertical dotted lines in Fig. 5, where α, β, and γ denote the 220–350, 80–220, and 20–80 K regions, respectively). As shown in the high temperature region α, term A is found to increase with the decreasing temperature for either medium voltage fits (0.1–0.3 V, empty squares) or high voltage fits (0.3–0.8 V, empty circles) from Eq. (10). By further linearly fitting the yielded A, we may obtain the ideality factors for medium and high voltage regimes as 1.19 and 1.93 from Eq. (11), respectively, which demonstrates that zone II in Fig. 4

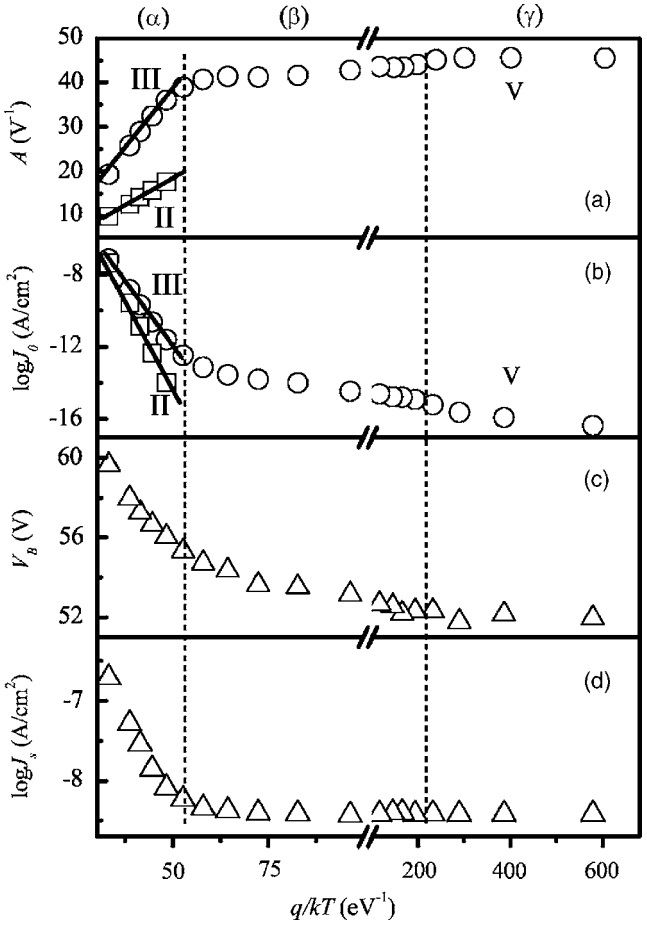

FIG. 5. Calculated parameters of (a) A and (b) J_0 at different temperatures, where empty circles and squares correspond to medium and high voltage fits by using Eqs. (10)–(12), and the numbers "II," "III," and "V" correspond to the zone designations in Fig. 4(a). (c) Breakdown voltage and (d) measured reverse current density vs q/kT. The solid curves are linear fitting results. The vertical dashed lines distinguish three temperature regions: (α) high temperature (220–350 K), (β) medium temperature (80–220 K), and (γ) low temperature (20–80 K).

is limited by the recombination current, while for zone III, diffusion current dominates. Such kind of behavior is consistent with the J-V behavior of normal diodes; however, it should be emphasized that the physical origin of the measured recombination current is on the nc-Si:H side of the depletion region. This argument can be further confirmed by the linear relationship between $\log(J_0)$ and q/kT [shown in Fig. 5(b), empty squares], which leads to the activation energy of 0.89 eV from Eq. (12), quite close to the half of the measured band gap of nc-Si:H (0.92 eV). As we know, there are two dominant effects that decide the recombination current,[35] the width of the depletion region and the defect level density near the midgap. In c-Si, the defect density is so small that can be neglected, while in the nc-Si:H layer, since about half of the film is composed of the a-Si:H tissue, the defect levels in the band gap are quasicontinuous. Therefore, it is reasonable that the recombination current occurs in the nc-Si:H side of the depletion region.

For temperature below 80 K, it is found that QCE and the tunneling govern the dark J-V behavior. When the applied forward bias is below the turn-on voltage (i.e., zone IV), electrons are confined in the nanodots, since they cannot be thermally activated into the extended state above the energy barrier [~60 meV (Ref. 12)]. With the bias increases beyond the turn-on voltage (i.e., zone V), the transport is still dominated by interband tunneling through the HJ interface, which can be evidenced by the temperature-independent parameter A illustrated in the low temperature region γ of Fig. 5(a). The deduced activation energy E_{ac} from Eq. (12) is about 100 meV, which is higher than that of the nanodot barrier but is still lower than the built-in potential on the nc-Si:H side of the HJ interface, leading to the tunneling dominant transport in zone V.

To further understand the transport properties, Figs. 5(c) and 5(d) illustrate the temperature dependence of the breakdown voltage V_b and measured reverse saturation current J_s at −10 V, respectively. It is well known that the breakdown voltage increases with the increasing temperature owing to the avalanche multiplication, whereas for the tunneling breakdown, it is just the opposite. Therefore, from Fig. 5(c), we may conclude that in the high temperature region α, the breakdown is of avalanche type, while below 80 K, it is a mixture of both avalanche and tunneling since the almost temperature-independent behavior of the breakdown voltage. As for the measured reverse saturation current J_s, it exhibits the same temperature profile as the calculated J_0. This kind of similarity in the slope of the curves also applies to Figs. 5(a)–5(d), which supports the temperature region partitions on the basis of the fitted parameter A, indicating the nontunneling and tunneling transport on the high and low temperature ends and transitional region in the middle. Moreover, former $C_0 \sim T$ result [Fig. 3(c)] also shows a sharp transition at 40 K, corresponding to the upper limit of the tunneling temperature region in J-V curve (80 K). The difference could be accounted for by the mechanism difference lying between the forward transport direction and the reverse one, and it also implies that the capacitance-temperature measurement is more sensitive to transition from nontunneling to tunneling, while J-V technique is more suitable for qualitative analysis of transport mechanisms.

IV. CONCLUSIONS

C-V analysis has revealed that the band discontinuity of the nc-Si:H(n)/c-Si(p) diode mainly exists on the valence-band side. An interface charge density on the order of 10^{11} cm^{-2} is estimated via the numerical C-V matching technique, and the low interface defect density has been demonstrated by the frequency insensitive C-f results. By dark J-V-T measurements, temperature- and bias-dependent transport mechanisms have been clarified by several separated zones marked on the J-V-T graph, and the extracted parameters indicate a transition from nontunneling to tunneling dominant transport from 350 to 20 K. Basic material parameters have also been carefully prepared by various optical and electrical measures, which are beneficial for the in-depth investigation into the nc-Si:H/c-Si HJ devices. Future work in prospect includes investigations on the heterostructure formed by the boron-doped p-type nc-Si:H and n-type c-Si, which has been shown to have potential applicability in solar cells.[36] However, inferred from recent studies on

a-Si:H(*p*)/*n*-Si(*n*) heterostructure,[37] nc-Si:H(*p*)/*c*-Si(*n*) HJ might have difference in the band discontinuity compared with the discussed nc-Si:H(*n*)/*c*-Si(*p*) one. Researches on the *J-V* characteristics of our HJs under illumination are also underway.

ACKNOWLEDGMENTS

This work was supported by the National Natural Science Foundation of China (Contract No. 10674094), National Major Basic Research Project of 2006CB921507, the Minister of Education of PCSIRT (Contract No. IRT0524), and the Shanghai Municipal Commission of Science and Technology Projects of 05DJ14003 and 06JC14039.

[1]Y. Hamakawa, J. Non-Cryst. Solids **352**, 863 (2006).
[2]A. T. Hatzopoulos, I. Pappas, D. H. Tassis, N. Arpatzanis, C. A. Dimitriadis, F. Templier, and M. Oudwan, Appl. Phys. Lett. **89**, 193504 (2006).
[3]W. Pan, J. J. Lu, J. Chen, and W. Z. Shen, Phys. Rev. B **74**, 125308 (2006).
[4]C. Y. Ng, T. P. Chen, M. Yang, J. B. Yang, L. Ding, C. M. Li, A. Du, and A. Trigg, IEEE Trans. Electron Devices **53**, 663 (2006).
[5]K. S. Cho, N.-M. Park, T.-Y. Kim, K.-H. Kim, and G. Y. Sung, Appl. Phys. Lett. **86**, 071909 (2005).
[6]G. Conibeer *et al.*, Thin Solid Films **511–512**, 654 (2006).
[7]S. Guha and J. Yang, J. Non-Cryst. Solids **352**, 1917 (2006).
[8]Y. L. He, C. Yin, G. Cheng, L. Wang, X. Liu, and G. Y. Hu, J. Appl. Phys. **75**, 797 (1994).
[9]Y. L. He, Y. Wei, G. Zheng, M. Yu, and M. Liu, J. Appl. Phys. **82**, 3408 (1997).
[10]H. Chen, W. Z. Shen, and W. S. Wei, Appl. Phys. Lett. **88**, 121921 (2006).
[11]X. Y. Chen, W. Z. Shen, H. Chen, R. Zhang, and Y. L. He, Nanotechnology **17**, 595 (2006).
[12]J. Chen, J. J. Lu, W. Pan, K. Zhang, X. Y. Chen, and W. Z. Shen, Nanotechnology **18**, 015203 (2007).
[13]Y. L. He, G. Y. Hu, M. B. Yu, M. Liu, J. L. Wang, and G. Y. Xu, Phys. Rev. B **59**, 15352 (1999).
[14]H. Matsuura and H. Okushi, in *Amorphous and Microcrystalline Semiconductor Devices*, edited by J. Kanicki (Artech House, Boston, 1992), Vol. II.
[15]X. Xu, J. Yang, A. Banerjee, S. Guha, K. Vasanth, and S. Wagner, Appl. Phys. Lett. **67**, 2323 (1995).
[16]M. Farrokh-Baroughi, C.-H. Lee, and S. Sivoththaman, J. Vac. Sci. Technol. A **24**, 821 (2006).
[17]S. Nomura, T. Iitaka, X. Zhao, T. Sugano, and Y. Aoyagi, Phys. Rev. B **59**, 10309 (1999).
[18]S. R. Forrest, in *Heterojunction Band Discontinuities: Physics and Device Applications*, edited by F. Capasso and G. Margaritondo (North-Holland, Oxford, 1987), Chap. 8.
[19]L. F. Marsal, J. Pallares, and X. Correig, J. Appl. Phys. **79**, 8493 (1996).
[20]K. Kamjoo, D. K. Nayak, J. S. Park, J. C. S. Woo, and K. L. Wang, J. Appl. Phys. **69**, 6674 (1991).
[21]P. Rosales-Quintero, A. Torres-Jacome, R. Murphy-Arteaga, and M. Landa-Vázquez, Semicond. Sci. Technol. **19**, 366 (2004).
[22]L.-W. Wang and A. Zunger, Phys. Rev. Lett. **73**, 1039 (1994).
[23]R. Tsu, D. Babic, and L. Ioriatti, Jr., J. Appl. Phys. **82**, 1327 (1997).
[24]F. Trani, D. Ninno, and G. Iadonisi, Phys. Rev. B **75**, 033312 (2007).
[25]A. Achiq, R. Rizk, F. Gourbilleau, R. Madelon, B. Garrido, A. Pérez-Rodríguez, and J. R. Morante, J. Appl. Phys. **83**, 5797 (1998).
[26]M. N. Islam and S. Kumar, J. Appl. Phys. **93**, 1753 (2003).
[27]R. L. Anderson, Solid-State Electron. **5**, 341 (1962).
[28]C. T. Sah and V. G. K. Reddi, IEEE Trans. Electron Devices **11**, 345 (1964).
[29]T. Unold, M. Rösch, and G. H. Bauer, J. Non-Cryst. Solids **266–269**, 1033 (2000).
[30]Y. Nemirovsky, G. Gordon, and D. Goren, J. Appl. Phys. **84**, 1113 (1998).
[31]H. Mimura and Y. Hatanaka, Appl. Phys. Lett. **50**, 326 (1987).
[32]J. M. Essick and J. D. Cohen, Appl. Phys. Lett. **55**, 1232 (1989).
[33]M. Farrokh Baroughi, R. Jeyakumar, Y. Vygranenko, F. Khalvati, and S. Sivoththaman, J. Vac. Sci. Technol. A **22**, 1015 (2004).
[34]H. C. Card, J. Appl. Phys. **50**, 2822 (1979).
[35]S. M. Sze, *Physics of Semiconductor Devices*, 2nd ed. (Wiley, New York, 1981).
[36]Z. Hu, X. Liao, H. Diao, Y. Cai, S. Zhang, E. Fortunato, and R. Martins, J. Non-Cryst. Solids **352**, 1900 (2006).
[37]I. Sakata, M. Yamanaka, and R. Shimokawa, Jpn. J. Appl. Phys., Part 2 **43**, L954 (2004).